Received: 13 October 2020 | Revised: 22 October 2020 | Accepted: 2 November 2020

DOI: 10.1002/prp2.693

INVITED REVIEW

Identification of an irreversible PPARγ antagonist with potent anticancer activity

Youyi Peng[1] | Qiang Zhang[2] | Robert M. Zielinski[3] | Richard D. Howells[4] | William J. Welsh[1,2]

[1]Biomedical Informatics Shared Resource, Cancer Institute of New Jersey, Rutgers, The State University of New Jersey, New Brunswick, NJ, USA

[2]Department of Pharmacology, Robert Wood Johnson Medical School, Rutgers, The State University of New Jersey, Piscataway, NJ, USA

[3]Graduate School of Biomedical Sciences, New Jersey Medical School, Rutgers, The State University of New Jersey, Newark, NJ, USA

[4]Department of Biochemistry & Molecular Biology, New Jersey Medical School, Rutgers, The State University of New Jersey, Newark, NJ, USA

Correspondence
Youyi Peng and William J. Welsh, Biomedical Informatics Shared Resource, Cancer Institute of New Jersey, Rutgers, The State University of New Jersey, 195 Little Albany Street, New Brunswick, NJ 08903, USA.
Emails: pengyo@cinj.rutgers.edu and welshwj@rwjms.rutgers.edu

Present address
Qiang Zhang, Intra-Cellular Therapies, Inc., 430 East 29th Street, New York, NY 10016, USA

Funding information
New Jersey Health Foundation, Grant/Award Number: IG-N4-16; NIH, Grant/Award Number: 1S10OD012346-01A1; Rutgers-Cancer Institute of New Jersey, Grant/Award Number: P30CA072720-5917

Abstract

Melanoma is responsible for most skin cancer deaths, and its incidence continues to rise year after year. Different treatment options have been developed for melanoma depending on the stage of the disease. Despite recent advances in immuno- and targeted therapies, advanced melanoma remains incurable and thus an urgent need persists for safe and more effective melanoma therapeutics. In this study, we demonstrate that a novel compound MM902 (3-(3-(bromomethyl)-5-(4-(*tert*-butyl) phenyl)-1H-1,2,4-triazol-1-yl) phenol) exhibited potent efficacies in inhibiting the growth of different cancer cells, and suppressed tumor growth in a mouse xenograft model of malignant melanoma. Beginning with MM902 instead of specific targets, computational similarity- and docking-based approaches were conducted to search for known anticancer drugs whose structural features match MM902 and whose pharmacological target would accommodate an irreversible inhibitor. Peroxisome proliferator-activated receptor (PPAR) was computationally identified as one of the pharmacological targets and confirmed by in vitro biochemical assays. MM902 was shown to bind to PPARγ in an irreversible mode of action and to function as a selective antagonist for PPARγ over PPARα and PPARδ. It is hoped that MM902 will serve as a valuable research probe to study the functions of PPARγ in tumorigenesis and other pathological processes.

KEYWORDS

anticancer, irreversible antagonist, melanoma, PPARγ

Abbreviations: COX, cyclooxygenase; DTT, dithiothreitol; FBS, fetal bovine serum; GST, gluthathione S-transferase; NSAID, nonsteroidal anti-inflammatory drug; NTI, naltrindole; PDE5, phosphodiesterase 5; PPARγ, peroxisome proliferator-activated receptor gamma; RXR, Retinoid X Receptor; SA/XL665, XL665-labeled streptavidin; SRC, steroid receptor coactivator; TR-FRET, time-resolved fluorescence resonance energy transfer.

This paper is dedicated to the memory of co-author Dr Richard D. (Rick) Howells, a dear friend, colleague, and inspiring research collaborator.

1 | INTRODUCTION

Melanoma is responsible for most skin cancer deaths, and its incidence continues to rise year after year. The American Cancer Society has estimated that 100 350 new melanoma cases would be diagnosed with 6850 deaths due to this disease across the US in 2020. Malignant melanoma, the most aggressive form of skin cancer, causes 80% of skin cancer-related deaths.[1] The treatment options for melanoma include surgery, immunotherapy, targeted therapy, chemotherapy, and radiation, depending on the stage of the disease.

Recent development of immunotherapy and targeted therapy has made a significant impact on the treatment of late-stage melanoma and the overall prognosis for these patients. BRAF and MEK targeted therapies (eg, dabrafenib, vemurafenib, trametinib, and cobimetinib) have demonstrated significant benefit in patients with BRAF V600 mutant advanced melanoma and remain viable first-line treatment options.[2] Nevertheless, these targeted therapies can lead to acquired drug resistance very quickly and eventually become ineffective in treating melanoma patients. Meanwhile, immune checkpoint inhibitors including PD-1 (nivolumab and pembrolizumab) and CTLA-4 (ipilimumab) antibodies have greatly improved the overall survival of patients with well-tolerated safety profiles.[3,4] However, in addition to their adverse side effects, these therapies can lead to either acquired drug resistance or low response rates in patients. Despite the advances in immunotherapy and targeted therapies, melanoma currently can be cured by surgical resection only if diagnosed early, and advanced melanoma remains incurable. Consequently, an urgent need for safe and more effective melanoma therapeutics persists.

Previously, we reported that naltrindole (NTI), a selective delta opioid receptor antagonist, inhibited human multiple myeloma cell growth in vitro (EC_{50} = 18.5 μmol/L) and exhibited efficacy in a mouse xenograft model, by interaction with non-opioid receptor targets.[5] Employing pharmacophore-based molecular modeling of NTI analogs, we have rationally designed and synthesized a series of trisubstituted triazoles as new delta opioid receptor ligands,[6,7] which in turn have led to the discovery of a novel compound MM902 I showing no appreciable binding affinity to opioid receptors (Figure 1). In this report, we demonstrate that MM902 inhibited the growth of various cancer cell lines in vitro and suppressed tumor growth in a mouse xenograft model of malignant melanoma. Similarity- and docking-based computational studies suggested that MM902 covalently binds to the ligand binding domain (LBD) of nuclear receptors. In vitro biochemical binding and functional assays further confirmed that MM902 acts as a peroxisome proliferator-activated receptor γ (PPARγ) selective antagonist in an irreversible mode of action. It is

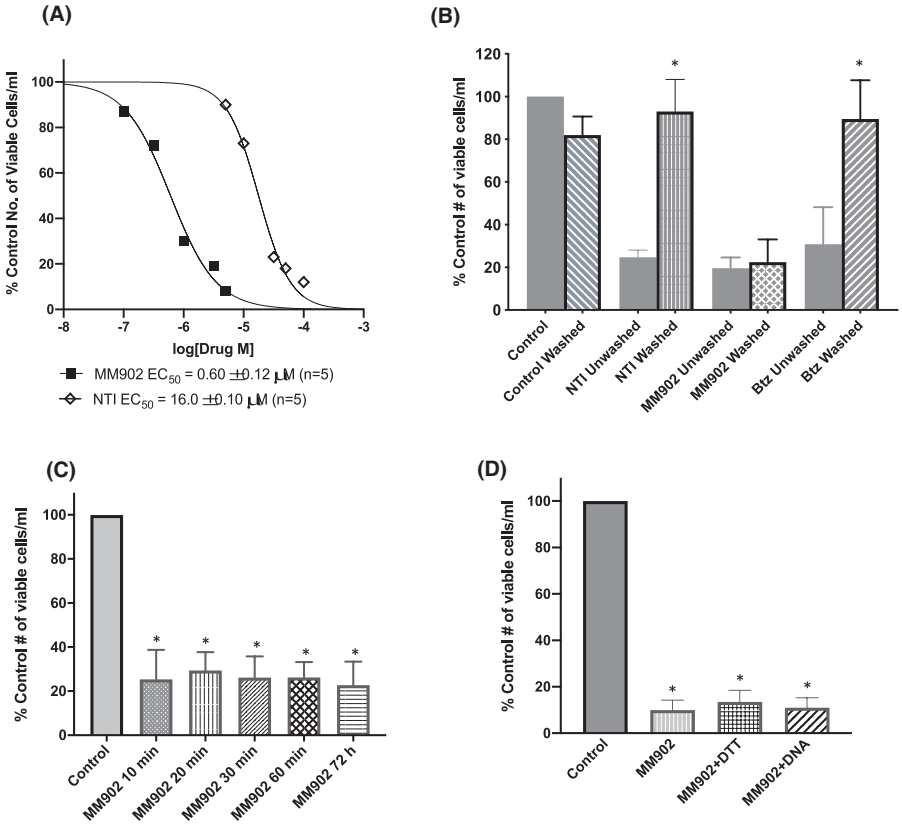

FIGURE 1 MM902 inhibits the growth of U266 multiple myeloma cell. A, Efficacy of MM902 to inhibit U266 cell growth in vitro. B, Washout effects on the inhibition of U266 cells by MM902 (Student *t*-test: washed vs unwashed treatments, $P < .05$). C, Time course of the irreversible inhibition of U266 cells by MM902 (Student *t*-test, treatment vs control, $P < .05$). D, Lack of effects of molar excess of DTT and DNA on the inhibition of U266 cell growth (Student *t*-test, treatment vs control, $P < .05$). Error bars represent standard error of mean (SEM, N = 4). Asterisks refer to statistically significant changes at $P < .05$, as described in the text. Btz, bortezomib

Chemistry

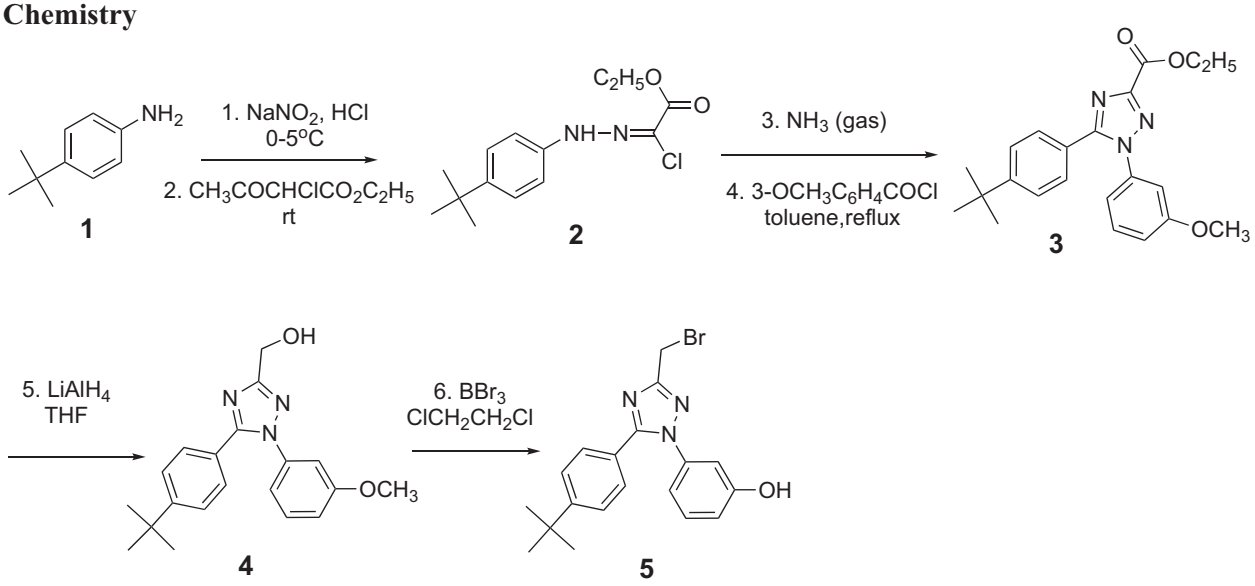

SCHEME 1 Synthesis of MM902

hoped that this study will encourage more interest in PPARγ antagonists such as MM902 as novel therapeutic treatments for cancer and other diseases.

2 | MATERIALS AND METHODS

2.1 | Chemistry

All reactions were carried out with anhydrous solvents in oven-dried and argon-charged glassware. Anhydrous solvents were freshly distilled and stored in 4 Å molecular sieves. All solvents used in workup, extraction procedures, re-crystallization process, and chromatography were used as received from commercial suppliers without further purification. All reagents were purchased from Sigma-Aldrich (St. Louis, MO).

Analytical thin layer chromatography was performed on precoated plastic backed plates (0.25-mm thickness) purchased from Sigma-Aldrich (Silica Gel 60 F254). Flash column chromatography was conducted with Silica Gel 60 (230-400 mesh) from Natland Co (Triangle Park, NC). HPLC was performed using the Waters ACQUITYTM HPLC system (Milford, MA), which was equipped with a Synergi 4u Fusion-RP80A column (2.0 mm × 50 mm) and a photodiode array detector. Samples were run under gradient conditions with CH_3CN/H_2O modified with 0.1% formic acid. MS and MS–MS were conducted on a Finnigan LCQ DUO Mass Spectrum from Thermo Fisher Scientific (Waltham, MA), and gas chromatographic analyses were performed on a Hewlett–Packard 6890 GC–MS instrument (Agilent Technologies, Santa Clara, CA) with an FID detector using 25 m × 0.20 mm capillary column with cross-linked methylsiloxane as a stationary phase. ^{1}HNMR spectra were recorded by a Brucker 400 MHz spectrometer (Billerica, MA) in deuterated DMSO (DMSO-d6) solution at room temperature, using TMS (0.00 parts per million [ppm]) as the internal standard and were reported in ppm. Abbreviations for signal coupling are as follows: s, singlet; d, doublet; t, triplet; q, quartet; m, multiplet; w, wide. Coupling constants (*J*) are reported in Hz.

MM902 was prepared as Scheme 1 with purity >95% under 254 nm. ^{1}HNMR (DMSO-d_6,400 MHz) δ 9.96 (s, 1H), 7.40 (dd, J = 6.2,7.4 Hz, 4H), 7.28 (t, J = 7.0 Hz, 1H), 6.89 (d, J = 6.8 Hz, 1H), 3.79 (m, 2H), 4.69 (s, 2H), 1.26 (s, 9H). (ESI) m/z 386.1, 388.1 $[M + H]^+$.

2.2 | Molecular modeling studies

All computational molecular modeling and docking studies were performed on an Intel Xeon CPU E5-2643 3.4 GHz processor with a memory of 64 GB RAM using the Molecular Operating Environment (MOE 2018.08, Chemical Computing Group, Montreal, QC, Canada), or GOLD (version 5.7.3) from the Cambridge Crystallographic Data Centre (CCDC, Cambridge, UK).[8]

Ligands were constructed with the Builder module in MOE, and the structures were geometry optimized by energy minimization with the MMFF94X force field and partial atomic charges. All X-ray crystallographic structures were downloaded from the PDB (www.rcsb.org) and processed in MOE using the Structure Preparation and Protonate 3D modules with default settings. All water molecules in the crystal structures were removed prior to the calculations. The PDB IDs are 6IJR and 3B0R (PPARγ),[9] 1MVC (Retinoid X Receptor α: RXRα),[10] and 1UDT and 1T9S (Phosphodiesterase 5: PDE5).[11,12]

GOLD was used for docking and covalent docking with the binding sites defined as the atoms within 10 Å radius around the centroids of the co-crystalized ligands. GoldScore was selected as the scoring and ranking function for all docking. Binding poses were exported to MOE for analyses.

2.3 | Cell culture

Human U266 multiple myeloma and LOX IMVI melanoma cells were obtained from the American Type Culture Collection (Manassas, VA) and National Cancer Institute (NCI), respectively. All cells were revived from frozen liquid nitrogen stocks and the adherent cell lines being grown were maintained in tissue culture flasks. These cells were cultured in suspension at 37°C in a humidified atmosphere containing 5% CO_2 in RPMI 1640 medium supplemented with 10% fetal bovine serum (FBS).

2.4 | Vi-cell determination of cell growth

The Vi-Cell from Beckman Coulter (Fullerton, CA) was used to determine cell growth. This instrument is an automated cell counter and viability analyzer that makes use of trypan blue exclusion staining combined with image-based analysis to determine the total number of viable cells and viability percentages. U266 cells were cultured in 12-well plates in the presence or absence of various concentrations of tested articles and appropriate controls at a cell density of approximately 100 000 cells/mL in order to construct dose-response curves. After 72 hours, 1.5 mL aliquots of cell culture media were collected and transferred to a Vi-Cell cuvette for Vi-Cell readings. EC_{50} values were determined by nonlinear regression of curves by plotting the log of the concentration of compounds used vs the number of viable cells/mL as determined the Vi-Cell using Prism 8.0 (Graph Pad Software Inc, San Diego, CA).

2.5 | Studies to determine the reversibility of inhibition

U266 multiple myeloma cells were incubated at 37°C in RPMI with 10% FBS for 1 hour with 50 μmol/L NTI, 10 nmol/L bortezomib, or 15 μmol/L MM902, followed by washout of the drugs, and then cells were incubated for 72 hours either with or without the re-addition of the drugs to the cell media prior to determining the number of viable cells/mL. In the experiment to study the time course of the irreversible inhibition, the U266 cells were incubated at 37°C in RPMI with 10% FBS for 10, 20, 30, or 60 minutes, followed by washout of the drug, prior to re-incubation for 72 hours of the washed samples compared with MM902 being present for the 72-hour period. Cell growth was determined by using the Vi-Cell cuvette described above.

Similar experiments were conducted to study if MM902 acts as a nonspecific alkylating agent. The U266 cells were incubated at 37°C in RPMI with 10% FBS for 72 hours in the presence of MM902 (15 μmol/L) with the addition of molar excesses of 1 mmol/L dithiothreitol (DTT), or with excess extracellular plasmid 25 μg/mL DNA. Cell growth was determined by using the Vi-Cell cuvette described above.

2.6 | DTP-NCI assays

MM902 was screened by the Developmental Therapeutics Program (DTP) at the NCI to test its cytotoxicity against the NCI-60 cancer cell lines, first at a single high dose of 10 μmol/L, and later at five descending doses. The dose-response assays were repeated two times.

MM902 was further evaluated for acute toxicity by the DTP. MM902 was dissolved in 100% DMSO and then injected intraperitoneally (i.p.) to each of three female mice at a dose of 400, 200, and 100 mg/kg, respectively. The mice were observed for a period of 2 weeks for apparent toxicity, including more than 20% of the body weight loss or other signs of significant toxicity.

The detailed assay information can be obtained from the NCI-DTP website (http://dtp.nci.nih.gov).

2.7 | KINOMEScan® kinase profiling

The scanEDGE℠ assay in the KINOMEscan® platform was performed by Eurofins DiscoveRx (Fremont, CA) against a panel of 97 human protein kinases to identify potential kinase targets for MM902. Primary screening was performed in duplicate at a single concentration of 10 μmol/L, which was followed by dose-response assays to determine binding affinities for targets showing promising inhibition by MM902 over a range of 3 nmol/L to 200 μmol/L. The results were reported as percent of control for the primary screen and as binding constants (K_d) for the follow-up screen.

2.8 | In vitro binding and functional assays

All radiolabeled binding assays, fluorescence enzymatic assays, and TR-FRET functional assays were performed by Eurofins Panlabs Discovery Services (Taipei, Taiwan). The AlphaScreen assays were performed by Eurofins Cerep (Celle-Lévescault, France). IC_{50} and EC_{50} values were determined by nonlinear regression of curves using the GraphPad Prism 8.0 software (GraphPad Software, La Jolla, CA).

2.8.1 | PPARγ radiolabeled binding assay

The binding assay was conducted in duplicate according to previously reported procedures.[13,14] The human recombinant PPARγ LBD expressed in insect cells was used in modified Tris-HCl buffer at pH 7.4. The protein (50 μL × 5 μmol/L in each well) was incubated with 5 nmol/L [^{3}H] rosiglitazone and 1 μg anti-gluthathione S-transferase (GST) antibody for 24 hours at 4°C. After incubation, the binding assay was terminated by addition of cold buffer. The mixture was then filtered through Whatman GF/B filters and washed with cold buffer. Radioactivity was recorded using the PerkinElmer TopCount liquid scintillation counter (PerkinElmer, Waltham, MA). Nonspecific receptor binding was measured in the presence of 10 μmol/L

unlabeled rosiglitazone (a known PPARγ agonist) which was used as a positive control in this assay.

2.8.2 | RXRα radiolabeled binding assay

The binding assay was conducted in duplicate according to previously reported procedures.[15] Human recombinant RXRα expressed in *Escherichia coli* cells (50 μL × 5 μmol/L in each well) was incubated with 5 nmol/L [^{3}H] 9-cis-retinoic acid in Tris-HCl buffer at pH 7.4 for 16 hours at 4°C. Nonspecific receptor binding was measured in the presence of 1 μmol/L unlabeled 9-cis-retinoic acid. The scintillation counter was used to measure the radioactivity. 9-Cis-retinoic acid was used as a positive control in this assay.

2.8.3 | RXRβ radiolabeled binding assay

Human recombinant RXRβ expressed in insect cells (50 μL × 5 μmol/L in each well) was incubated in duplicate with 5 nmol/L [^{3}H] 9-cis-retinoic acid in Tris-HCl buffer at pH 7.4 for 24 hours at 4°C, according to previously reported procedures.[16] Nonspecific receptor binding was measured in the presence of 10 μmol/L unlabeled 9-cis-retinoic acid. The scintillation counter was used to measure the radioactivity. 9-Cis-retinoic acid was used as a positive control in this assay.

2.8.4 | COX-1 fluorescence assay

Human recombinant cyclooxygenase 1 (COX-1) expressed in baculovirus infected Sf9 cells was used in this assay according to previously reported procedures.[17] Test compounds and vehicles were preincubated with COX-1 (at 0.4 μg/mL in each well) in Tris-HCl buffer at pH 8.0 for 15 minutes at 25°C in duplicate. The reaction was initiated by addition of 3 μmol/L arachidonic acid and 100 μmol/L Ampliflu™ Red, and then incubated for another 3 minutes. The fluorescence of resorufin was analyzed with the Tecan M1000Pro fluorescence spectrometer (Tecan Trading AG, Zürich, Switzerland) using an excitation wavelength of 535 nm and an emission wavelength of 590 nm. Indomethacin was used as a positive control in this assay.

2.8.5 | COX-2 fluorescence assay

Human recombinant cyclooxygenase 2 (COX-2) expressed in insect infected Sf9 cells was used in this assay according to previously reported procedures.[18] Test compounds and vehicles were preincubated with COX-2 (at 0.4 μg/mL in each well) in modified Tris-HCl buffer at pH 8.0 for 15 minutes at 25°C in duplicate. The reaction was initiated by addition of 3 μmol/L arachidonic acid and 100 μmol/L Ampliflu™ Red, and then incubated for another 3 minutes. The fluorescence of resorufin was analyzed with the Tecan Infinite 200Pro fluorescence spectrometer (Tecan Trading AG, Zürich, Switzerland) using an excitation wavelength of 535 nm and an emission wavelength of 590 nm. Rofecoxib was used as a positive control in this assay.

2.8.6 | TR-FRET functional assays

The PPARγ functional assays were conducted using homogeneous time-resolved (TR) fluorescence technology by measuring fluorescence resonance energy transfer (FRET).[19] Briefly, the human recombinant PPARγ-LBD tagged with GST (1 nmol/L) was incubated with an Europium-labeled anti-GST antibody (2 nmol/L), testing samples and DMSO controls, followed by addition of biotinylated steroid receptor coactivator (SRC), XL665-labeled streptavidin (SA/XL665, 20 nmol/L) in Tris-HCl buffer at pH 7.4 for 16 hours at 4°C. The buffer consisted of 50 mmol/L Tris-HCl, 0.1% BSA, 0.125% CHAPS, 3 mmol/L DTT, 30 μmol/L EDTA. The fluorescence signals were measured with a PHERAstar FS Microplate Reader (BMG Labtech, Ortenberg, Germany) using an excitation wavelength of 337 nm and emission wavelengths of 620 and 665 nm.

2.8.7 | Agonist mode

Fluorescence responses from 10 μmol/L rosiglitazone were used as the 100% activation controls. The 0% activation control contains 1% DMSO in the final assay vehicle in place of an agonist and is used to determine the lower end of the assay in the agonist mode, or to determine the maximal inhibition (100% inhibition) as well in the antagonist mode. Percentage (%) of activation for testing samples was calculated by the formula below. Known PPARγ agonist rosiglitazone was used as the positive control.

2.8.8 | Antagonist mode

Tagged PPARγ and its coactivator were pre-incubated with test samples followed by agonist challenge at the EC_{80} concentrations: 1 μM rosiglitazone used as EC_{80} controls. Percentage (%) of inhibition for test samples was calculated using the formula below. Known PPARγ antagonist GW9662 was used as the positive control.

$$\text{Emission Ratio (ER)} = \frac{\text{Fluorescein Emission at 665 nm}}{\text{Fluorescein Emission at 620 nm}},$$

$$\%\,\text{Activation - Agonist Mode} = \left\{ \frac{\text{ER}_{\text{Sample \% Act}} - \text{ER}_{0\,\%\,\text{Act Ctrl}}}{\text{ER}_{100\,\%\,\text{Act Ctrl}} - \text{ER}_{0\,\%\,\text{Act Ctrl}}} \right\} \times 100,$$

$$\%\,\text{Inhibition - Antagonist Mode} = \left\{1 - \frac{ER_{\text{Sample}\,\%\ \text{Act}} - ER_{0\,\%\ \text{Act Ctrl}}}{ER_{\text{EC80 Ctrl}} - ER_{0\,\%\ \text{Act Ctrl}}}\right\} \times 100.$$

2.9 | AlphaScreen functional assays

Evaluation of the antagonistic activity of MM902 at three human PPAR nuclear receptors was conducted by Eurofins Cerep using the AlphaScreen detection method to measure its effects on agonist-induced light emission signals.[20-22]

2.9.1 | PPARα antagonist mode

Human PPARα-LBD tagged with histidine (25 nmol/L protein) was pre-incubated for 5 minutes at 22°C in the buffer containing 20 mmol/L HEPES/NaOH (pH 7.4), 80 mmol/L NaCl, 0.08% Tween 20, 0.8 mmol/L DTT and 0.08% BSA, in the presence of the incubation buffer (basal and stimulated control), a known PPARα antagonist GW7647, or MM902. Subsequently, 100 nmol/L GW7647, 25 nmol/L biotin-tagged-PGC1 alpha coactivator and 0.4 μg fluorescence acceptor (anti-histidine antibody coupled-beads) were added and the mixture was incubated for 30 minutes at 22°C. For the basal control, GW7647 was omitted from the reaction mixture. Fluorescence donor (streptavidin coupled-beads) was then added to the mixture at a final concentration of 0.4 μg. After 120 minutes incubation at 22°C, the luminesce signals were measured using an excitation wavelength of 680 nm and emission wavelengths of 520 and 620 nm with an EnVision Microplate Reader (Perkin Elmer, Waltham, MA). The results were expressed as percent (%) inhibition of the control response to 100 nmol/L GW7647. MM902 was tested at the concentrations of 0.05 to 100 μmol/L in duplicates.

2.9.2 | PPARδ antagonist mode

Human PPARδ-LBD tagged with histidine (1.7 μL/mL protein) was pre-incubated for 5 minutes at 22°C in the buffer containing 20 mmol/L HEPES/NaOH (pH 7.4), 80 mmol/L NaCl, 0.08% Tween 20, 0.8 mmol/L DTT and 0.08% BSA, in the presence of the incubation buffer (basal and stimulated control), a known PPARδ antagonist GSK0660, or MM902. Subsequently, 10 nmol/L GW0742, 50 nmol/L biotin-tagged-C33 coactivator and 0.4 μg fluorescence acceptor (anti-histidine antibody coupled-beads) were added and the mixture was incubated for 30 minutes at 22°C. For the basal control, GW0742 was omitted from the reaction mixture. Fluorescence donor (streptavidin coupled-beads) was then added to the mixture at a final concentration of 0.4 μg. After 120 minutes incubation at 22°C, the luminesce signals were measured using an excitation wavelength of 680 nm and emission wavelengths of 520 and 620 nm with an EnVision Microplate Reader. The results were expressed as percent (%) inhibition of the control response to 10 nmol/L GW0742. MM902 was tested at the concentrations of 0.05 to 100 μmol/L in duplicates.

2.9.3 | PPARγ antagonist mode

Human PPARγ-LBD tagged with histidine (50 nmol/L protein) was pre-incubated for 5 minutes at 22°C in the buffer containing 20 mmol/L HEPES/NaOH (pH 7.4), 80 mmol/L NaCl, 0.08% Tween 20, 0.8 mmol/L DTT and 0.08% BSA, in the presence of the incubation buffer (basal and stimulated control), a known PPARγ antagonist GW9662, or MM902. Subsequently, 1 μmol/L rosiglitazone, 50 nmol/L biotin-tagged-TRAP220 coactivator and 0.4 μg fluorescence acceptor (anti-histidine antibody coupled-beads) were added and the mixture was incubated for 30 minutes at 22°C. For the basal control, rosiglitazone is omitted from the reaction mixture. Fluorescence donor (streptavidin coupled-beads) was then added to the mixture at a final concentration of 0.4 μg. After 120 minutes incubation at 22°C, the luminesce signals were measured using an excitation wavelength of 680 nm and emission wavelengths of 520 and 620 nm with an EnVision Microplate Reader. The results were expressed as a percent (%) inhibition of the control response to 1 μmol/L rosiglitazone. MM902 was tested at the concentrations of 0.05 to 100 μmol/L in duplicate.

2.10 | Mouse xenograft study

This study was performed in collaboration with Washington Biotechnology, Inc (Baltimore, MD). Guidelines from the Institutional Animal Care and Use Committee were followed to handle the animals. SCID CB17 mice (female, 5-6 weeks old) from Charles River Laboratories (Wilmington, MA) were used in this study. All mice were ear tagged for identification purposes. Upon arrival, animals were examined to ensure that they were healthy, and then housed in autoclaved solid floor polycarbonate cages.

LOX-IMVI melanoma cells were cultured in a 25-cm^2 flask containing RPMI 1640 media supplemented with 10% FBS and incubated at 37°C in humidified atmosphere of 5% CO_2. As cells reached 80% confluence, cultures were expanded to 175 cm^2 flasks until sufficient cells were available for injection. 2.5 million cancer cells in PBS with 20% Matrigel were injected subcutaneously into the right flank of each mouse. Once tumors were palpable, the mice were randomized into three groups of six mice. Control mice were treated intraperitoneally (i.p.) with vehicle (DMSO) and treatment groups with MM902 once daily at a dose of 50 and 25 mg/kg. Tumor sizes and body weights were measured three times a week, and tumor volumes were calculated using the formula for a hemiellipsoid: $\text{Tumor Volume} = \frac{1}{2}(\text{length} \times \text{width} \times \text{height})$.

2.11 | Statistical analysis

The statistical significance of mean values was determined by using a Student *t*-test implemented in Prism 8.0. Differences with *P* values < .05 were considered statistically significant.

2.12 | Nomenclature of targets and ligands

Key protein targets and ligands in this article are hyperlinked to corresponding entries in http://www.guidetopharmacology.org, the common portal for data from the IUPHAR/BPS Guide to PHARMACOLOGY and are permanently archived in the Concise Guide to PHARMACOLOGY 2019/20.[23,24]

3 | RESULTS

3.1 | Chemistry

The synthesis of the novel analog MM902 (3-(3-(bromomethyl)-5-(4-(*tert*-butyl) phenyl)-1H-1,2,4-triazol-1-yl) phenol) is depicted in Scheme 1. Reaction of 4-tert-butylbenzenamine **1** with $NaNO_2$ in 2.0 mol/L HCl at 5°C gave diazonium salt, which was reacted with ethyl-2-chloro-3-oxobutanoate to yield intermediate **2**. Amination of **2** with ammonia produced amidrazone in 100% yield typically within 2 hours The 1,2,4-triazole core ring was then closed by refluxing of amidrazone with 3-methoxybenzoyl chloride in toluene to give the key intermediate **3**. The ethyl ester in **3** was then quantitively converted to alcohols using $LiAlH_4$ as a reducing reagent. The hydroxyl group in compound **4** was converted to bromide at the same time when compound **4** was cleaved to phenol **5** by excessive BBr_3. Yield was greater than 85% for this step.

3.2 | MM902 inhibited U266 multiple myeloma cells in an irreversible mode

Naltrindole is a highly potent and selective delta opioid receptor antagonist and has been widely used as a research probe in the studies of pain. Previously, employing pharmacophore-based molecular modeling, we have rationally designed and synthesized series of trisubstituted triazoles as novel delta opioid receptor ligands.[6,7] More recently, we reported that NTI inhibited the growth of human U266 cancer cells in vitro and in vivo in a mouse xenograft model, by an opioid receptor independent mechanism.[5] Consequently, several of the triazole analogs, including MM902, were tested for their effects on the growth of human U266 cells. MM902 exhibited no appreciable binding affinity for the opioid receptors due to the absence of the basic nitrogen atom, an essential pharmacophore for opioid ligands. However, as shown for Figure 1A, MM902 exhibited much more potent inhibition of U266 cancer cell growth with $EC_{50} = 0.60 \pm 0.12$ μmol/L than NTI with $EC_{50} = 16.0 \pm 0.10$ μmol/L, which motivated further studies on this compound.

The structure of MM902 contains a bromoalkyl group, which is a common feature in many irreversible alkylating agents. Consequently, a pertinent question is whether MM902 is acting in an irreversible manner in inhibiting the U266 cell growth or the inhibition of cell growth itself was irreversible once initiated? The inhibition irreversibility of MM902 was compared to that of NTI and bortezomib in washout experiments (Figure 1B). NTI is a reversible ligand and has been shown to inhibit U266 cells, while bortezomib is a reversible proteasome inhibitor approved by the FDA for the treatment of multiple myeloma patients.[25] U266 cells were incubated in the presence of all three compounds (MM902 at 15 μmol/L, NTI at 50 μmol/L, and bortezomib at 10 nmol/L) for 1 hour followed by a washout procedure. The cells were then incubated for 72 hours either with or without the re-addition of the drugs to the cell media prior to determining the number of viable cells/mL.

In this experiment, the groups without re-addition of drugs are named "washed", while the counterparts with re-addition of drugs are named "unwashed". In the unwashed samples, all three compounds exhibited potent inhibition in the growth of U266 cells in comparison with the vehicle control ($P < .0001$). The numbers of viable U266 cells were reduced to 25% by NTI, 20% by MM902 and 31% by bortezomib at the tested concentrations relative to the control. However, after removal of the drugs post a 1-hour incubation, the inhibitory effects by NTI and bortezomib were abolished in the washed groups and were significantly different from those in the unwashed groups ($P < .05$), suggesting that the inhibition of cell growth itself was reversible after initiated and both drugs act in a reversible mode of action. Conversely, the inhibitory effects by MM902 in the washed and unwashed groups were not significantly different ($P = .64$), indicating removal of the drug could not reverse the inhibition in cell growth, which is consistent with an irreversible mode of action.

After MM902 was shown to act irreversibly in inhibiting the U266 multiple myeloma cell growth, another experiment was performed to study the time course of the irreversibility (Figure 1C). The U266 cells were incubated in the presence of MM902 (15 μmol/L) for 10 minutes, 20 minutes, 30 minutes, 1 hour, and 72 hours. After only 10 minutes of exposure to MM902, there was a significant inhibition (75%) of cell growth vs control ($P < .0001$). However, at time points longer than 10 minutes, the inhibition effects were not significantly different from $t = 10$ minutes ($P = .92$), indicating that even a 10 minutes incubation was sufficient for MM902 to exert irreversible inhibition of U266 cell growth.

The next question is whether MM902 acts nonspecifically as a classical alkylating agent or selectively for one or more specific targets? Similar experiments were performed with the addition of molar excesses of the sulfhydryl reducing agent, DTT, or with excess extracellular plasmid DNA (Figure 1D). The U266 cells were incubated in the presence of MM902 (15 μmol/L) with and without molar excesses of 1 mM DTT or 25 μg/mL of DNA for 72 hours. MM902 alone exhibited 88% inhibition of the U266 cell growth. With the addition of excess DTT, the inhibitory action of MM902 on U266 cell growth was not changed significantly ($P = .29$). Similar results were obtained with the addition of excess plasmid DNA. The changes in the U266 cell growth are not significant ($P = .68$). DTT is a reducing agent and widely used to reduce disulfide bonds. The presence of DTT in the media will free the cysteines (Cys) in proteins, which makes Cys available for alkylation by other agents like MM902 in this experiment. Meanwhile, most classical alkylating agents like alkyl

sulfonates, nitrosoureas, and ethylenimines, interact with the N7 atom of guanine base of DNA to form a covalent DNA adduct. It is reasonable to assume that the inhibition of U266 cancer cell growth by MM902 will be greatly reduced or blocked by the presence of excess DTT and DNA if MM902 acts as a nonspecific alkylating agent. However, neither excess DTT nor DNA significantly reduced the inhibition effects by MM902, suggesting this irreversibility was not due to rampant alkylation, but rather targeted reaction. Taken together, the evidence supports the premise that MM902 acts via an irreversible and targeted mechanism.

3.3 | MM902 exhibited potent growth inhibition in NCI-60 screen

Since it demonstrated moderate potent inhibition (EC_{50} = 0.6 μmol/L) in U266 multiple myeloma cells, MM902 was submitted to the NCI-60 screen for cytotoxicity on a wide panel of cancers, which includes cancer cells from leukemia, melanoma, lung, colon, CNS, ovary, kidney, prostate, and breast cancers. The screening results of MM902 against all cancer cells are shown in Figures S1 and S2. MM902 exhibited cytotoxicity with GI_{50} values of single-digit μmol/L against most cancer cells. For a subset of cancer cells, MM902 demonstrated very strong inhibition (with GI_{50} < 0.5 μmol/L) in the cell growth assays (Table 1). For example, MM902 exhibited GI_{50} values of 154 nmol/L and 351 nmol/L in leukemia CCRF-CEM and SR cells, 355 and 275 nmol/L in ovarian IGROV1 and renal 786-0 cells, and 170 and 349 nmol/L in nonsmall cell lung cancer NCI-H522 and melanoma MALME-3M cells. More interestingly, MM902 potently inhibited human melanoma cells LOX-IMVI with a GI_{50} value of 27 nmol/L, which motivated further studies to evaluate its safety and efficacy in vivo.

3.4 | MM902 showed no acute toxicity in mice

Given the encouraging results in the NCI-DTP screen, MM902 was further evaluated for acute toxicity by the NCI-DTP in mice. MM902 in 100% DMSO was injected intraperitoneally to each of three female mice at a dose of 400, 200, and 100 mg/kg, respectively. The mice were observed for a period of 2 weeks for apparent toxicity and weight loss. At the end of the 2-week period, all mice were still alive, and none exhibited more than 20% of the body weight loss or other signs of significant toxicity (Table 2), suggesting MM902 is not toxic in this acute study.

TABLE 1 Selected GI_{50} data from MM902's NCI-60 screen

Cancer panel	Cell line	GI_{50} (nmol/L ± SEM)
Leukemia	CCRF-CEM	154 ± 6
	SR	351 ± 142
NSCLC	NCI-H522	170 ± 31
Melanoma	LOX-IMVI	27 ± 7
	MALME-3M	349 ± 92
Ovarian	IGROV1	355 ± 34
Renal	786-0	275 ± 88

Note: GI_{50} is the concentration of a compound that causes 50% growth inhibition, relative to the no-drug control. Assays were repeated twice.

3.5 | MM902 inhibited tumor growth in melanoma xenograft model

As shown above, MM902 exhibited the most potent inhibition against the LOX-IMVI human melanoma cell line in the NCI-60 screen with GI_{50} = 27 nmol/L. This melanoma cell line is widely used as an in vitro model system to study tumor metastasis and to test for chemosensitivity to potential anti-cancer compounds. It was deemed interesting to evaluate MM902 in a mouse LOX-IMVI melanoma cancer xenograft model for its in vivo efficacy in suppressing tumor growth. To achieve this, SCID mice were subcutaneously inoculated bilaterally in the hind flanks with human LOX-IMVI melanoma cancer cells. When palpable tumors were present, mice were injected (i.p.) with vehicle or MM902 daily at 25 and 50 mg/kg for 10 days (N = 6 each group). The initial research plan was for 3 weeks on treatment; however, the LOX-IMVI melanoma cancer grew very fast and the tumor sizes quickly reached 2000 mm^3 in the control group at day 10, which resulted in the early termination of this study. In this first proof of concept experiment, a large number (2.5 million) melanoma cancer cells were subcutaneously injected to the mice, which may result in the quick growth of cells within a shortened time. Future studies with reduced inoculated cell number should be performed to prolong the period of tumor growth for better observations.

Tumor volumes in the control and drug treated mice were measured biweekly. As shown in Figure 2A, MM902 reduced the tumor volumes in a dose dependent way. At the low (25 mg/kg) and high (50 mg/kg) doses, the averaged tumor volume was reduced by 25% and 70%, respectively, after a 10-day treatment. The reduction in the tumor volume by 70% in the high dose group was statistically significant (P = .05) compared with the vehicle control group. Body weight losses in drug-treated mice at both doses and at all time points were well below 20% recommended as the upper limit for such animal studies,[26] suggesting that MM902 was well tolerated (Figure 2B). Even at the high dose of 50 mg/kg, the maximum body weight loss in mice was only 15% on days 3 and 6. It is plausible that MM902's nature of irreversible inhibition may partially account for the weight loss. However, initial acute toxicity studies (albeit in a single mouse) by NCI-DTP suggested that MM902 was not overtly toxic at doses up to 400 mg/kg. Therefore, it remains to be determined to what degree the weight loss is treatment related, or due to the effects of compromised metabolism by the malignant melanoma in the mice. Changes in doses and schedules with less inoculated cells are suggested for future studies.

TABLE 2 Results for acute toxicity study by NCI-DTP

Dose (mg/kg)	Schedule	Conc. (mg/mL)	Injection volume (μL/g Body Weight)	Survival/total on day 14
100	QD X 1, day 0	200	0.5	1/1
200	QD X 1, day 0	200	1.0	1/1
400	QD X 1, day 0	200	2.0	1/1

Abbreviation: NCI-DTP, National Cancer Institute-Developmental Therapeutics Program.

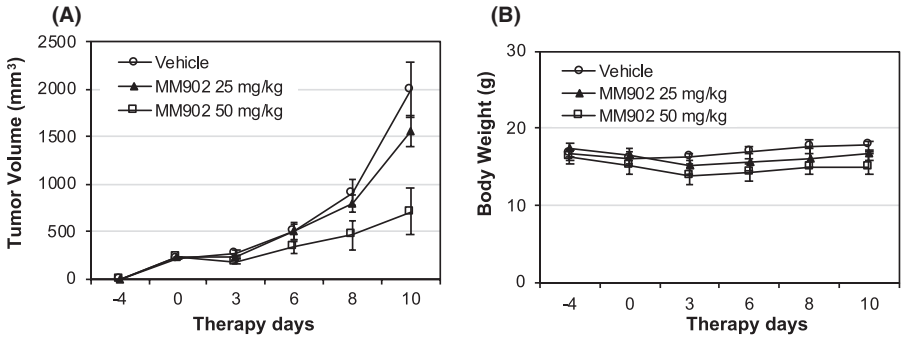

FIGURE 2 Effect of MM902 on melanoma tumor growth in a murine SCID/human LOX-IMVI xenograft model. Tumor sizes (A) and body weights (B) were measured three times a week. SCID CB17 mice were used in this study (N = 6). Error bars represent SEMs. At 50 mg/kg, the reduction in tumor volume by 70% was statistically significant (Student *t*-test $P < .05$)

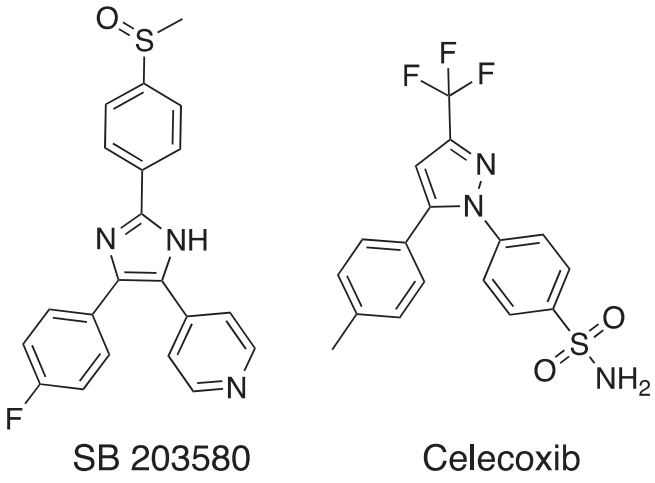

FIGURE 3 Structures of SB203580 and Celecoxib

3.6 | Computer-aided target identification for MM902

As described above, MM902 demonstrated potent inhibition of cancer cell growth in vitro, as well as efficacy in a melanoma xenograft mouse model and no acute toxicity in the NCI-DTP mouse study in vivo. Significant effort was then undertaken to identify its pharmacological target(s) employing computational approaches in drug similarity and receptor docking. We have been aware that MM902 structure bears a likeness to the p38 MAP kinase inhibitor SB 203 580 and the COX-2 selective inhibitor celecoxib (Figure 3), which served as starting points for our computational studies.

3.6.1 | Kinome profiling

The structural similarity between MM902 and SB203580 prompted us to test MM902 in the scanEDGE℠ panel of Eurofins DiscoveRx for kinase profiling, which includes 97 kinases distributed throughout the AGC, CAMK, CMGC, CK1, STE, TK, TKL, lipid, and atypical kinase families, plus important mutant forms.

The profiling results at 10 μmol/L for the entire panel, shown in Figure 4, revealed that MM902 is able to bind to 18 of 97 kinases at 30% to 55% relative to the control, either orthosterically or allosterically. The tabulated results are shown in Supporting Information (Table S1). Of these, it is especially interesting that MM902 demonstrated binding of 37% and 55% to the B-Raf (V600E) mutant form and the IKK-alpha, respectively, since the B-Raf mutant has been found in approximately 50% of malignant melanoma tumors,[27,28] and the IKK/NFγB pathway is activated in melanoma cancer cells.[29] Dose-response curve assays to determine the binding constants for these two kinases were followed over a concentration range of 3 to 200 μmol/L; however, MM902 did not show significant binding to either kinase at those concentrations and, therefore, the binding constants were not determined. The results for the single concentration assay were evidently false positives. This study indicates that these kinases are likely not the pharmacological targets for MM902.

3.6.2 | Molecular modeling of PPAR and RXR

Further studies were conducted to seek the biological targets of MM902, which shares structurally similarity to celecoxib, a COX-2

selective nonsteroidal anti-inflammatory drug (NSAID) that is prescribed to treat pain and inflammation associated with various diseases. Celecoxib has demonstrated anti-proliferative activities in certain types of cancer preclinically and clinically.[30] It was deemed worthwhile to determine if celecoxib displayed inhibition activity in our U266 cell growth assay, and to compare its potency and efficacy to those of MM902. This would provide insight into the pharmacological targets of MM902 that are responsible for its mechanism of action. Celecoxib was studied in the U266 cell growth assay at concentrations from 0.3 to 30 μmol/L and was found to inhibit cell growth with EC_{50} = 15.9 ± 3.1 μmol/L, significantly less potent than MM902 (EC_{50} = 0.60 μmol/L).

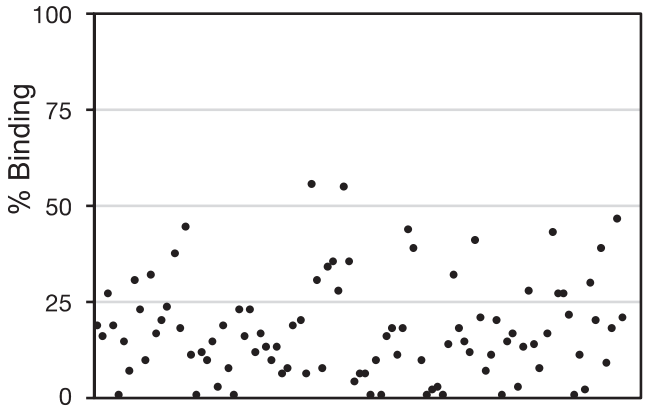

FIGURE 4 Kinase profiling in the scanEDGE℠ panel

Meanwhile, a careful literature review suggested that the anti-proliferative activities of celecoxib were independent of its inhibition of the COXs.[31] For example, another COX-2 inhibitor, rofecoxib, although structurally related to celecoxib, exhibits similar potency (IC_{50}) toward inhibition of COX-2 but much less anti-proliferative activity than celecoxib in both COX-2 positive and negative cell lines.[32] Therefore, it is highly unlikely that COX-2 is the pharmacological target of MM902. Later, MM902 was tested in fluorescence-based activity assays of human COX-1 and COX-2 in Tris-HCl buffer at pH 8.0 at 25°C according to previously reported methods.[17,18] The fluorescence for COX-1 and COX-2 was analyzed with a Tecan M1000Pro and 200Pro spectrometer using an excitation wavelength of 535 nm and an emission wavelength of 590 nm, respectively. MM902 lacked any apparent inhibition of either target at the concentration of 1 μmol/L (Figure 5A), which confirmed our hypothesis that MM902 does not target the COXs.

According to the literature, multiple cellular targets have been proposed as the COX-independent mechanisms for the anti-proliferative activities of NSAIDs, including phosphodiesterase 5 (PDE5), nuclear receptors like PPARγ and RXR, and kinases like IKK and AMPK.[31] However, our previous kinase profiling in the scanEDGE℠ panel had suggested that kinases including IKK and MARKs (homologs of AMPK in the same CAMKL subfamily) are unlikely to be the pharmacological targets for MM902 (Figure 4; Table S1).

Since MM902 contains a bromoalkyl group and was indicated to act in a targeted irreversible mode by the wash-out experiment in the U266 multiple myeloma cells (Figure 1B,D), a potent nucleophile

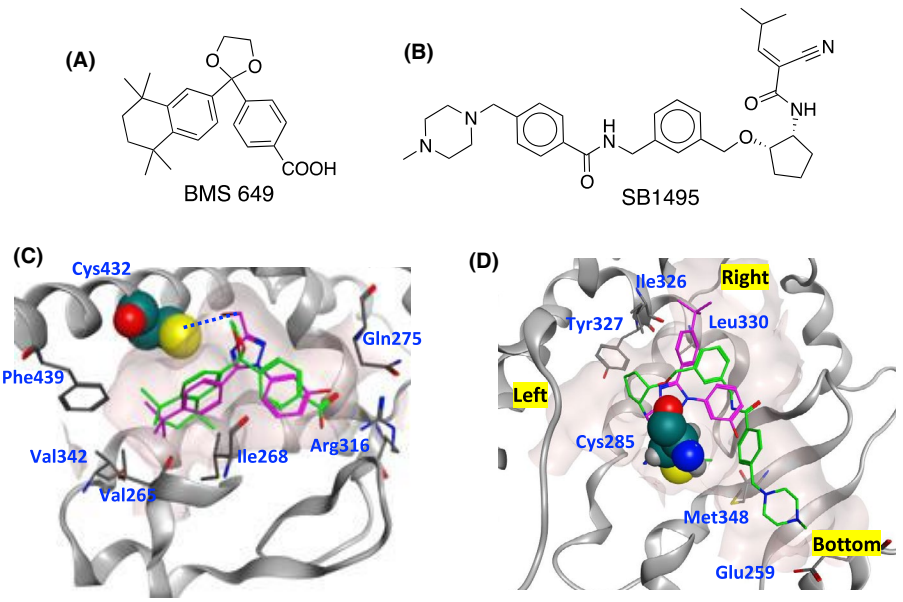

FIGURE 5 Docking-based identification of binding targets for MM902. A, Structure of BMS 649. B, Structure of SB1495. C, Predicted binding pose of MM902 (magenta) in the ligand binding pocket of RXRα (1MVC). The blue dashed line indicates a potential covalent bond between the ligand and receptor. D, Predicted binding pose of MM902 (magenta) in the ligand binding pocket of PPARγ (6IJR). Protein structures are depicted as gray ribbons while the ligands are rendered as sticks. BMS 649 and SB1495 are rendered as green sticks. Putatively important residues are shown as sticks and labeled accordingly. Cys432 and Cys285 are rendered as space-filled models and colored by atom type. The ligand binding pockets are shown as light pink molecular surfaces. Three sub-pockets (Left, Right and Bottom) in PPARγ's ligand binding pocket are shown in yellow boxes and labeled accordingly

such as cysteine (Cys) in the binding site of the targets was considered to be essential to form a covalent bond with the ligand. Although weaker nucleophiles like serine (Ser) could potentially work, our attention initially focused on the Cys residue. The crystal structures of PDE5, PPARγ, and RXR were surveyed to check if there are any Cys residues in the binding sites.

For PDE5, sildenafil (PDB ID: 1UDT) and GMP (PDB ID: 1T9S) bound crystal structures were selected for the analysis.[11,12] Cys residues in PDE5 were found to be structurally far away from the ligand binding site and none were located within 5Å of the co-crystalized ligands sildenafil and GMP (Figure S3), suggesting PDE5 is unlikely to be the target to form a covalent bond with MM902.

For RXRs, the BMS 649-bound RXRα crystal structure (PDB ID:1MVC) was selected for visual analysis and molecular docking.[10] BMS 649 (Figure 5A) is a pan-RXR agonist and binds to a pocket delineated by the helical residues H3, H5, H11, and β-strand in the LBD of RXRα. As shown in Figure 5C, the tetramethyl-naphthalenyl group of BMS 649 is located in a hydrophobic cavity surrounded by Val265 (H3), Ile268 (H3), Val342, Phe439 (H11), while the carboxylate moiety engages in an anionic interaction with Arg316 (H5). Meanwhile, the dioxolan group is positioned very close to Cys432 (H11), a strong nucleophile that could potentially form a covalent bond with an electrophile on ligands. This Cys residue is also conserved in RXRβ (Cys503). Covalent docking of MM902 using GOLD into the ligand binding pocket of the RXRα structure revealed a tight fit: the *tert*-butyl-phenyl and phenolic groups of MM902 are overlapped nicely with the tetramethyl naphthalenyl and benzoate groups of BMS 649, and the bromomethyl of MMM902 is seated very close to Cys432 of RXRα, enabling the possible formation of a covalent bond between MM902 and the receptor.

For PPARγ, the SB1495-bound PPARγ crystal structure (PDB ID: 6IJR) was selected for this study. SB1495 (Figure 5B) is a covalent antagonist for PPARγ and its cyanoacrylamide moiety forms a covalent bond with Cys285 on the helix H3 of PPARγ (Figure 5C).[9] The ligand-binding pocket of PPARγ is in a Y-shaped with a large volume, which could accommodate diverse ligands including GW9662[33] and SR1664.[34] The left arm of the Y-shaped pocket consists of a mix of hydrophobic and polar residues, and the right arm of the Y is lined by hydrophobic residues (Ile326 and Leu330). The bottom arm of the Y-shaped pocket is extended to the helix H2′ and Ω loop, surrounded by both hydrophobic (Met348) and polar residues (Glu259). Docking of MM902 into the ligand binding pocket the PPARγ structure revealed it could fit into the right and bottom arms with its *tert*-butyl-phenyl positioned in the hydrophobic right arm and the phenolic group sitting in the bottom arm. The bromomethyl group of MMM902 is positioned very close to Cys285 on PPARγ, which increases its likelihood to form a covalent bond between the ligand and receptor.

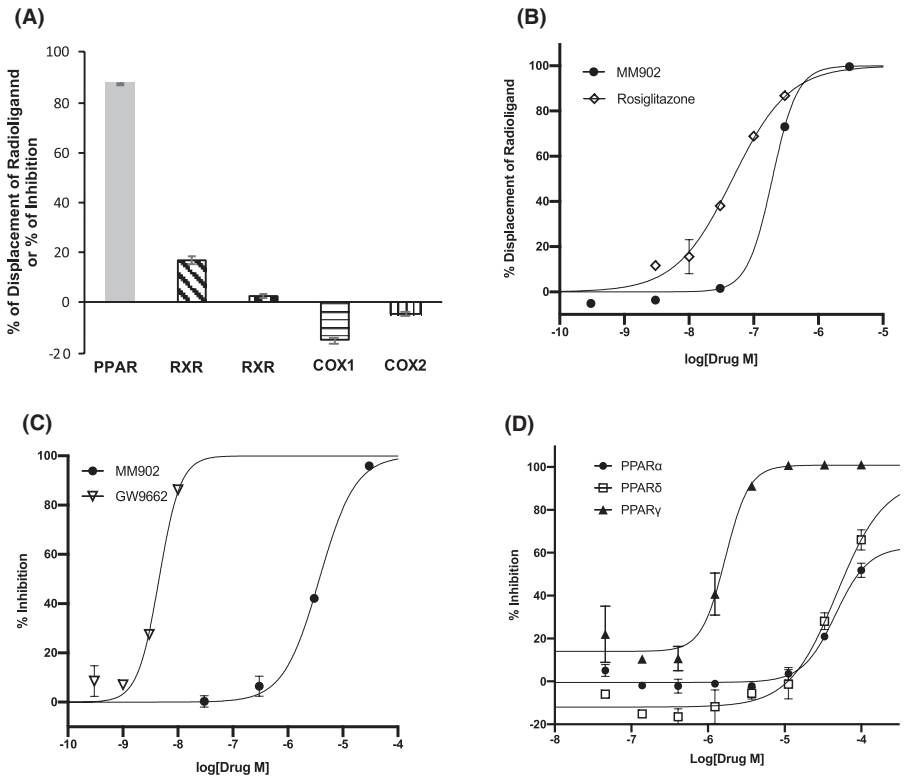

FIGURE 6 Identification of pharmacological targets for MM902. A, In vitro screening results at 1 μmol/L of MM902. B, Radiolabeled binding results for PPARγ. K_i values for MM902 and Rosiglitazone are 0.14 μmol/L and = 0.047 μmol/L. C, TR-FRET functional assay results for PPARγ. IC_{50} values for MM902 and GW9662 are 3.72 μmol/L and 4.52 nmol/L. D, AlphaScreen functional assay results for MM902. IC_{50} values for three human PPAR receptors are 1.68 μmol/L (PPARγ), 46.04 μmol/L (PPARα) and 48.01 μmol/L (PPARδ). Error bars represent SEMs. Rosiglitazone: PPARγ agonist; GW9662: PPARγ antagonist

Based upon the results from the molecular modeling and covalent docking, it was reasonable to hypothesize that RXRs (α and β) and PPARγ could be the potential pharmacological targets for MM902, which was validated by in vitro and cellular assays of these receptors.

3.7 | MM902 was confirmed experimentally as a PPARγ antagonist

In order to experimentally evaluate the hypothesis from the aforementioned molecular modeling studies, radiolabeled binding assays of human PPARγ and RXR (α and β) were then performed using previous reported methods.[15,16] Briefly, the LBDs of human PPARγ and RXR (α and β) were incubated in the Tris-HCl buffer at pH = 7.4 under 4°C for 16-24 hours using radioligands [^{3}H] rosiglitazone and [^{3}H] 9-cis-retinoic acid, respectively. After incubation, the radioactivity was recorded using the TopCount liquid scintillation counter. At the concentration of 1 μmol/L (Figure 6A), MM902 exhibited 88% binding to PPARγ compared with only 16% for RXRα and 3% for RXRβ, indicative of considerably more potent affinity to PPARγ than to RXRα and RXRβ. Follow-up dose-response assays were conducted to determine the binding constant for PPARγ over a range of concentrations from 0.03 to 30 μmol/L. As shown in Figure 6B, MM902 binds tightly to the receptor with a binding constant K_i = 0.14 μmol/L, thereby supporting our hypothesis based on our modeling studies that PPARγ is at least one of the primary pharmacological targets for MM902. Although rigid-receptor docking suggests that MM902 preferred the ligand-binding pocket of RXRα over PPARγ, results from the radiolabeled binding assays suggest the opposite. We reasoned that this inconsistency may be partially explained by the more spacious binding pocket of PPARγ (Figure 5D), which would offer the receptor and ligands greater flexibility to adopt optimal binding poses and subsequently more potent binding affinities.

Next, TR-FRET functional assays were then conducted for PPARγ to study whether MM902 activates or antagonizes the receptor according to the reported method.[19] Briefly, the human recombinant PPARγ-LBD tagged with GST was incubated with a Europium-labeled anti-GST antibody and MM902, followed by addition of biotinylated coactivator SRC, and XL665-labeled streptavidin in the Tris-HCl buffer at pH 7.4. The fluorescence signals were measured with a PHERAstar FS Microplate Reader using an excitation wavelength of 337 nm and emission wavelengths of 620 and 665 nm. MM902 was tested at concentrations of 0.03 to 30 μmol/L. In the agonist mode, the % activation of MM902 was compared to the reference compound rosiglitazone that was normalized to 100%. In this mode, the known PPARγ agonist rosiglitazone exhibited an EC_{50} of 0.041 μmol/L, while MM902 failed to show any apparent increase in the fluorescence responses even at the highest concentration 30 μmol/L, indicating it does not activate the association of PPARγ to its coactivator and, therefore, does not act as an agonist for the receptor. On the other hand, in the antagonist mode, MM902 exhibited significant inhibition of agonist (rosiglitazone)-induced fluorescence responses with IC_{50} = 3.72 μmol/L (Figure 6C), indicating MM902 acts as an antagonist for PPARγ.

In order to evaluate the selectivity of MM902 for the three human PPARs, its antagonistic effects on these receptors (α, δ, and γ) were measured using the previously described AlphaScreen method.[20-22] Briefly, the LBDs of recombinant human PPARs (α, δ, and γ) tagged with histidine were pre-incubated in the HEPES buffer with MM902 for 5 minutes, followed by addition of a known agonist (eg, rosiglitazone for PPARγ), biotin-tagged coactivator and anti-histidine antibody coupled-beads as the fluorescence acceptor. After incubation for 30 minutes, the fluorescence donor (streptavidin coupled-beads) was added to the mixture. Subsequently, the luminescence signals were measured using an EnVision Microplate Reader. Binding of agonists (eg, rosiglitazone) to the PPARs (eg, PPARγ) brings the fluorescence beads into proximity, which results in a cascade of chemical reactions to produce greatly amplified signals. MM902 exhibited much more potent inhibition of agonist-induced luminescence responses on PPARγ (IC_{50} = 1.68 μmol/L) than on PPARα (IC_{50} = 46.04 μmol/L) and PPARδ (IC_{50} = 48.01 μmol/L) (Figure 6D). Taken together, these results reveal that MM902 functions as a selective antagonist for PPARγ over PPARα and PPARδ.

4 | DISCUSSION

Target-based drug discovery begins with knowledge of a molecular target together with a specific ligand-binding site. Libraries of small-molecule compounds are then screened using high-throughput computational (in silico) and/or experimental (in vitro) methods to identify and rank "hits" whose structures are presumed to be complementary in shape and polarity to the target's ligand-binding pocket. This process is typically repeated and refined until a manageable series of "drug leads" is obtained for subsequent analyses using more elaborate structural biology and in vitro/in vivo studies. In the present case, the traditional drug discovery process is reversed. Beginning with the drug MM902 instead of specific targets, we employed computational similarity- and docking-based approaches to search for known antiproliferative drugs whose structural features match MM902 and whose pharmacological target would accommodate an irreversible (covalent) inhibitor. The evidence suggests that the inhibitory activity of MM902 on the growth of cancer cells results from irreversible antagonism of PPARγ with a binding constant (K_i) of 0.14 μmol/L and functional IC_{50} = 3.72 μmol/L (TR-FRET assay) and IC_{50} = 1.68 μmol/L (AlphaScreen assay). Although MM902 appeared to exhibit different degrees of potency in the in vitro radiolabeled binding (K_i) and in cell growth inhibition assays (GI_{50}), it is not uncommon that anticancer agents show much higher potency in cell growth assays than in radiolabeled binding assays. For example, paclitaxel, an anticancer agent used to treat many types of cancer, showed the IC_{50} value in the range of low μmol/L in radiolabeled tubulin binding assay but very potent GI_{50} values (<0.1 nmol/L) in cancer cell growth inhibition assay.[35] Sequence and structural analyses in the ligand binding pocket of PPARγ identified an essential residue Cys285 that putatively could form a covalent bond with the bromomethyl group on

MM902. Future mass spectrometry or X-ray crystallographic studies are necessary to confirm the covalent binding and to reveal the ligand-receptor interactions at the molecular level.

PPAR receptors (α, δ, and γ) belong to the superfamily of nuclear receptors,[36] and have been shown to play essential roles in metabolism and tumorigenesis.[37] PPARγ agonists (eg, thiazolidinediones) have been reported to exhibit antiproliferative effects in diverse cancer cells in vitro and in vivo,[38-40] and have entered clinical trials as anticancer therapeutics.[37,41] However, they have shown little therapeutic efficacy in clinical trials for different cancers.[42] In fact, retrospective analyses of patients with diabetes have suggested an increased risk of developing bladder cancer and melanoma associated with the chronic use of antidiabetic thiazolidinediones.[43,44] Consistent with these observations, the PPARγ agonist rosiglitazone has been shown to promote tumor cell growth via the induction of paracrine signaling in metastatic melanoma cells.[1] On the other hand, recently the PPARγ antagonists GW9662 and SR1664 were shown to inhibit the development of prostate cancer[45] and to sensitize cancer cells to cytotoxic chemotherapy,[46] respectively. Here we show another example that PPARγ antagonist MM902 could inhibit the growth of different cancer cells in vitro and in vivo. However, the inhibition effect by MM902 could possibly be attributed to all three PPAR receptors, though MM902 exhibited much stronger antagonistic activity on PPARγ (IC50 = 1.68 μmol/L) than on PPARα (IC_{50} = 46.04 μmol/L) and PPARδ (IC_{50} = 48.01 μmol/L). In addition, we must consider the possibility that MM902 may bind to other potential targets that modulate cell proliferation and growth.

Malignant melanoma, just like other cancers, is a highly heterogeneous tumor that exhibits widely varied expression of PPARγ. Recently Pich et al[1] quantified the expression levels of PPARγ in patient-resected melanoma and in a variety of melanoma cell lines, and found up to 64-fold difference between the lowest and highest expression. Unfortunately, it is unclear if this study included the LOX-IMVI melanoma cell line. Our observation that MM902 was efficacious both in vitro and in vivo in inhibiting cell and tumor growth of LOX-IMVI melanoma suggests elevated expression of PPARγ in this cancer cell line. Further RNA sequencing studies in the future would confirm this line of reasoning.

Targeted therapies and immunotherapies have demonstrated significant benefit in patients with BRAF V600 mutant advanced melanoma and greatly improved the overall survival of patients. Nevertheless, they can lead to either acquired drug resistance or low response rates in patients of melanoma. As a result, combination of targeted therapies and immunotherapies has been developed to overcome the drug resistance and achieve better-tolerated safety profiles.[3,4] For example, melanoma patients treated with the combination of vemurafenib and cobimetinib have achieved a higher objective response, longer progression-free survival and overall survival compared with vemurafenib alone.[47] There are many ongoing preclinical and clinical studies that are exploring diverse combinations of targeted therapies and immune checkpoint inhibitors in patients with BRAF-mutated metastatic melanoma. MM902, as a novel irreversible antagonist for PPARγ, represents a viable candidate for such combination studies with targeted therapies (BRAF and MEK inhibitors) and immunotherapies in vitro and in vivo to evaluate its ability to provide additive or synergistic effects in inhibiting the melanoma cancer cell growth.

Compared with reversible counterparts, irreversible ligands might improve effectiveness toward specific diseases and achieve higher specificity for pharmacological targets. Due to these notable advantages, several irreversible covalent drugs have already been approved by the FDA for multiple clinical indications, including pain, diabetes, and cancer.[48,49] However, the inherent reactivity and resulting toxicity of irreversible ligands limit their clinical applications. In our study, MM902 demonstrated good safety in the NCI-DTP acute toxicity studies at doses up to 400 mg/kg, however, weight loss was observed in the mouse xenograft study compared with the vehicle control group at certain time points. More studies are necessary to evaluate the toxic effects of MM902, when used alone or in combination with other anticancer agents. Nevertheless, MM902 represents a valuable research tool to study the functions of PPARs in tumorigenesis and other pathological processes.

In summary, we demonstrate here that MM902 inhibited the growth of various cancer cell lines in vitro and suppressed tumor growth in a mouse xenograft model of malignant melanoma. Computational similarity- and docking-based approaches have suggested that PPARγ is a pharmacological target for MM902, which was confirmed by in vitro biochemical assays. MM902 was demonstrated to bind to PPARγ by an irreversible mode of action and to function as a selective antagonist for PPARγ over PPARα and PPARδ. Further in vivo efficacy studies in a murine SCID/human LOX-IMVI xenograft model revealed that MM902 suppressed melanoma tumor growth in a dose-dependent manner, viz., by 70% at the highest dose tested (50 mg/kg). It is contemplated that this study will encourage further interest in PPARγ antagonists as novel therapeutic treatments for melanoma and other forms of cancer.

ACKNOWLEDGEMENTS

The authors thank the DTP of the NCI of the United States for performing the NCI-60 screen and acute toxicity assays. This research has been supported in part by a grant from the New Jersey Health Foundation (IG-N4-16), and from Rutgers-Cancer Institute of New Jersey Biomedical Informatics Shared Resource of the (P30CA072720-5917). We gratefully acknowledge access to the High Performance Computing facilities and support of the computational STEM at the Rutgers Office of Advanced Research Computing (OARC, URL: http://oarc.rutgers.edu). We also acknowledge the computational resources made accessible to the Perceval Linux cluster operated by OARC under NIH 1S10OD012346-01A1. We also want to acknowledge the assistance provided by Dr Vivian Bellofatto at the New Jersey Medical School of Rutgers. The authors declare no competing financial interests.

DISCLOSURES

The authors declare no competing financial interests.

AUTHOR CONTRIBUTIONS

Y. Peng, RD Howells, W. J. Welsh: Conception and design. Y. Peng, Q. Zhang, R. M. Zielinski, RD Howells, W. J. Welsh: Development of methodology. Y. Peng, RD Howells, W. J. Welsh: Acquisition of data (provided animals, provided facilities, etc). Y. Peng, RD Howells: Analysis and interpretation of data (eg, statistical analysis, biostatistics, computational analysis). Y. Peng, Q. Zhang, R. M. Zielinski, W. J. Welsh: Writing, review, and/or revision of the manuscript. Y. Peng: Administrative, technical, or material support (ie, reporting or organizing data, constructing databases). Y. Peng, RD Howells, W. J. Welsh: Study supervision.

DATA AVAILABILITY STATEMENT

All data generated during the course of the work in this manuscript will be made available upon request.

ORCID

Youyi Peng https://orcid.org/0000-0003-4797-995X
Robert M. Zielinski https://orcid.org/0000-0002-5275-1450

REFERENCES

1. Pich C, Meylan P, Mastelic-Gavillet B, et al. Induction of paracrine signaling in metastatic melanoma cells by PPARgamma agonist rosiglitazone activates stromal cells and enhances tumor growth. *Cancer Res*. 2018;78:6447-6461.
2. Cerchia C, Lavecchia A. Small molecule drugs and targeted therapy for melanoma: current strategies and future directions. *Curr Med Chem*. 2017;24:2312-2344.
3. Babacan NA, Eroglu Z. Treatment options for advanced melanoma after anti-PD-1 therapy. *Curr Oncol Rep*. 2020;22:38.
4. Smalley KS, Eroglu Z, Sondak VK. Combination therapies for melanoma: a new standard of care? *Am J Clin Dermatol*. 2016;17:99-105.
5. Mundra JJ, Terskiy A, Howells RD. Naltrindole inhibits human multiple myeloma cell proliferation in vitro and in a murine xenograft model in vivo. *J Pharmacol Exp Ther*. 2012;342:273-287.
6. Peng Y, Zhang Q, Arora S, et al. Novel delta opioid receptor agonists exhibit differential stimulation of signaling pathways. *Bioorg Med Chem*. 2009;17:6442-6450.
7. Zhang Q, Keenan SM, Peng Y, et al. Discovery of novel triazole-based opioid receptor antagonists. *J Med Chem*. 2006;49:4044-4047.
8. Jones G, Willett P, Glen RC, Leach AR, Taylor R. Development and validation of a genetic algorithm for flexible docking. *J Mol Biol*. 1997;267:727-748.
9. Jang JY, Kim H, Kim HJ, Suh SW, Park SB, Han BW. Structural basis for the inhibitory effects of a novel reversible covalent ligand on PPARgamma phosphorylation. *Sci Rep*. 2019;9:11168.
10. Egea PF, Mitschler A, Moras D. Molecular recognition of agonist ligands by RXRs. *Mol Endocrinol*. 2002;16:987-997.
11. Sung BJ, Hwang KY, Jeon YH, et al. Structure of the catalytic domain of human phosphodiesterase 5 with bound drug molecules. *Nature*. 2003;425:98-102.
12. Zhang KY, Card GL, Suzuki Y, et al. A glutamine switch mechanism for nucleotide selectivity by phosphodiesterases. *Mol Cell*. 2004;15:279-286.
13. Ferry G, Bruneau V, Beauverger P, et al. Binding of prostaglandins to human PPARgamma: tool assessment and new natural ligands. *Eur J Pharmacol*. 2001;417:77-89.
14. Fujimura T, Sakuma H, Ohkubo-Suzuki A, Aramori I, Mutoh S. Unique properties of coactivator recruitment caused by differential binding of FK614, an anti-diabetic agent, to peroxisome proliferator-activated receptor gamma. *Biol Pharm Bull*. 2006;29:423-429.
15. Peet DJ, Doyle DF, Corey DR, Mangelsdorf DJ. Engineering novel specificities for ligand-activated transcription in the nuclear hormone receptor RXR. *Chem Biol*. 1998;5:13-21.
16. Allenby G, Bocquel MT, Saunders M, et al. Retinoic acid receptors and retinoid X receptors: interactions with endogenous retinoic acids. *Proc Natl Acad Sci U S A*. 1993;90:30-34.
17. Swinney DC, Mak AY, Barnett J, Ramesha CS. Differential allosteric regulation of prostaglandin H synthase 1 and 2 by arachidonic acid. *J Biol Chem*. 1997;272:12393-12398.
18. Riendeau D, Charleson S, Cromlish W, Mancini JA, Wong E, Guay J. Comparison of the cyclooxygenase-1 inhibitory properties of non-steroidal anti-inflammatory drugs (NSAIDs) and selective COX-2 inhibitors, using sensitive microsomal and platelet assays. *Can J Physiol Pharmacol*. 1997;75:1088-1095.
19. Zhou G, Cummings R, Li Y, et al. Nuclear receptors have distinct affinities for coactivators: characterization by fluorescence resonance energy transfer. *Mol Endocrinol*. 1998;12:1594-1604.
20. Duncan JG, Fong JL, Medeiros DM, Finck BN, Kelly DP. Insulin-resistant heart exhibits a mitochondrial biogenic response driven by the peroxisome proliferator-activated receptor-alpha/PGC-1alpha gene regulatory pathway. *Circulation*. 2007;115:909-917.
21. Rieck M, Meissner W, Ries S, Muller-Brusselbach S, Muller R. Ligand-mediated regulation of peroxisome proliferator-activated receptor (PPAR) beta/delta: a comparative analysis of PPAR-selective agonists and all-trans retinoic acid. *Mol Pharmacol*. 2008;74:1269-1277.
22. Yang W, Rachez C, Freedman LP. Discrete roles for peroxisome proliferator-activated receptor gamma and retinoid X receptor in recruiting nuclear receptor coactivators. *Mol Cell Biol*. 2000;20:8008-8017.
23. Alexander SPH, Cidlowski JA, Kelly E, et al. THE CONCISE GUIDE TO PHARMACOLOGY 2019/20: nuclear hormone receptors. *Br J Pharmacol*. 2019;176(Suppl 1):S229-S246.
24. Harding SD, Sharman JL, Faccenda E, et al. The IUPHAR/BPS guide to PHARMACOLOGY in 2018: updates and expansion to encompass the new guide to IMMUNOPHARMACOLOGY. *Nucleic Acids Res*. 2018;46:D1091-D1106.
25. Curran MP, McKeage K. Bortezomib: a review of its use in patients with multiple myeloma. *Drugs*. 2009;69:859-888.
26. Morton DB. A systematic approach for establishing humane endpoints. *ILAR J*. 2000;41:80-86.
27. Cheng L, Lopez-Beltran A, Massari F, MacLennan GT, Montironi R. Molecular testing for BRAF mutations to inform melanoma treatment decisions: a move toward precision medicine. *Mod Pathol*. 2018;31:24-38.
28. Hayward NK, Wilmott JS, Waddell N, et al. Whole-genome landscapes of major melanoma subtypes. *Nature*. 2017;545:175-180.
29. Demchenko YN, Kuehl WM. A critical role for the NFkB pathway in multiple myeloma. *Oncotarget*. 2010;1:59-68.
30. Toloczko-Iwaniuk N, Dziemianczyk-Pakiela D, Nowaszewska BK, Celinska-Janowicz K, Miltyk W. Celecoxib in cancer therapy and prevention—review. *Curr Drug Targets*. 2019;20:302-315.
31. Gurpinar E, Grizzle WE, Piazza GA. COX-independent mechanisms of cancer chemoprevention by anti-inflammatory drugs. *Front Oncol*. 2013;3:181.
32. Waskewich C, Blumenthal RD, Li H, Stein R, Goldenberg DM, Burton J. Celecoxib exhibits the greatest potency amongst cyclooxygenase (COX) inhibitors for growth inhibition of COX-2-negative hematopoietic and epithelial cell lines. *Cancer Res*. 2002;62:2029-2033.

33. Leesnitzer LM, Parks DJ, Bledsoe RK, et al. Functional consequences of cysteine modification in the ligand binding sites of peroxisome proliferator activated receptors by GW9662. *Biochemistry*. 2002;41:6640-6650.
34. Choi JH, Banks AS, Kamenecka TM, et al. Antidiabetic actions of a non-agonist PPARgamma ligand blocking Cdk5-mediated phosphorylation. *Nature*. 2011;477:477-481.
35. Arora S, Wang XI, Keenan SM, et al. Novel microtubule polymerization inhibitor with potent antiproliferative and antitumor activity. *Cancer Res*. 2009;69:1910-1915.
36. Rosen ED, Spiegelman BM. PPARgamma: a nuclear regulator of metabolism, differentiation, and cell growth. *J Biol Chem*. 2001;276:37731-37734.
37. Zhao L, Zhou S, Gustafsson JA. Nuclear receptors: recent drug discovery for cancer therapies. *Endocr Rev*. 2019;40:1207-1249.
38. Sarraf P, Mueller E, Jones D, et al. Differentiation and reversal of malignant changes in colon cancer through PPARgamma. *Nat Med*. 1998;4:1046-1052.
39. Sarraf P, Mueller E, Smith WM, et al. Loss-of-function mutations in PPAR gamma associated with human colon cancer. *Mol Cell*. 1999;3:799-804.
40. Tsubouchi Y, Sano H, Kawahito Y, et al. Inhibition of human lung cancer cell growth by the peroxisome proliferator-activated receptor-gamma agonists through induction of apoptosis. *Biochem Biophys Res Commun*. 2000;270:400-405.
41. Kulke MH, Demetri GD, Sharpless NE, et al. A phase II study of troglitazone, an activator of the PPARgamma receptor, in patients with chemotherapy-resistant metastatic colorectal cancer. *Cancer J*. 2002;8:395-399.
42. Frohlich E, Wahl R. Chemotherapy and chemoprevention by thiazolidinediones. *Biomed Res Int*. 2015;2015:845340.
43. Ferrara A, Lewis JD, Quesenberry CP Jr, et al. Cohort study of pioglitazone and cancer incidence in patients with diabetes. *Diabetes Care*. 2011;34:923-929.
44. Soccio RE, Chen ER, Lazar MA. Thiazolidinediones and the promise of insulin sensitization in type 2 diabetes. *Cell Metab*. 2014;20:573-591.
45. Tew BY, Hong TB, Otto-Duessel M, et al. Vitamin K epoxide reductase regulation of androgen receptor activity. *Oncotarget*. 2017;8:13818-13831.
46. Khandekar MJ, Banks AS, Laznik-Bogoslavski D, et al. Noncanonical agonist PPARgamma ligands modulate the response to DNA damage and sensitize cancer cells to cytotoxic chemotherapy. *Proc Natl Acad Sci U S A*. 2018;115:561-566.
47. Ascierto PA, McArthur GA, Dreno B, et al. Cobimetinib combined with vemurafenib in advanced BRAF(V600)-mutant melanoma (coBRIM): updated efficacy results from a randomised, double-blind, phase 3 trial. *Lancet Oncol*. 2016;17:1248-1260.
48. Ghosh AK, Samanta I, Mondal A, Liu WR. Covalent inhibition in drug discovery. *ChemMedChem*. 2019;14:889-906.
49. Zhang T, Hatcher JM, Teng M, Gray NS, Kostic M. Recent advances in selective and irreversible covalent ligand development and validation. *Cell Chem Biol*. 2019;26:1486-1500.

SUPPORTING INFORMATION

Additional supporting information may be found online in the Supporting Information section.

How to cite this article: Peng Y, Zhang Q, Zielinski RM, Howells RD, Welsh WJ. Identification of an irreversible PPARγ antagonist with potent anticancer activity. *Pharmacol Res Perspect*. 2020;e00693. https://doi.org/10.1002/prp2.693